Terahertz eld enhancement to the MV/cm regime in a tapered parallel plate waveguide

Iwaszczuk, Krzysztof; Andryieuski, Andrei; Lavrinenko, Andrei; Zhang, X.-C. ; Jepsen, Peter Uhd

Published in:
Optics Express

Link to article, DOI:
10.1364/OE.20.008344

Publication date:
2012

Document Version
Publisher's PDF, also known as Version of record

Terahertz field enhancement to the MV/cm regime in a tapered parallel plate waveguide

K. Iwaszczuk,[1,*] **A. Andryieuski,**[1] **A. Lavrinenko,**[1] **X.-C. Zhang,**[2] **and P. U. Jepsen**[1]

[1]*DTU Fotonik, Technical University of Denmark, DK-2800 Kgs. Lyngby, Denmark*
[2]*The Institute of Optics, University of Rochester, Rochester, NY, 14627-0186 USA*
[*]*kiwa@fotonik.dtu.dk*
www.terahertz.dk

Abstract: We investigate field enhancement properties of a tapered parallel plate waveguide for ultrashort terahertz (THz) pulses. We use two independent methods, air biased coherent detection inside the waveguide and free-space electro-optic sampling, respectively, which enables a calibrated, quantitative measurement of the field strength at the output of the waveguide. Field enhancement factors greater than 20 are demonstrated and record-high field strengths of > 1.4 MV/cm are reached. We find an excellent agreement between the two independent methods of field measurement and a numerical 3D full-vectorial time-domain simulations.

OCIS codes: (230.7370) Waveguides; (300.6495) Spectroscopy, terahertz; (320.7160) Ultrafast technology Femtosecond phenomena.

References and links

1. P. U. Jepsen, D. G. Cooke, and M. Koch, "Terahertz spectroscopy and imaging - modern techniques and applications," Laser Photon. Rev. **5**, 124–166 (2011).
2. J. B. Baxter and G. W. Guglietta, "Terahertz spectroscopy," Anal. Chem. **83**, 4342–4368 (2011).
3. M. I. Stockman, "Nanofocusing of optical energy in tapered plasmonic waveguides," Phys. Rev. Lett. **93**, 137404 (2004).
4. S. A. Maier, S. R. Andrews, L. Martin-Moreno, and F. J. Garcia-Vidal, "Terahertz surface plasmon-polariton propagation and focusing on periodically corrugated metal wires," Phys. Rev. Lett. **97**, 176805 (2006).
5. A. R. Davoyan, V. V. Popov, and S. A. Nikitov, "Giant terahertz near-field enhancement by two-dimensional plasmons," arXiv:1109.3943v2 (2011).
6. M. A. Seo, H. R. Park, S. M. Koo, D. J. Park, J. H. Kang, O. K. Suwal, S. S. Choi, P. C. M. Planken, G. S. Park, N. K. Park, Q. H. Park, and D. S. Kim, "Terahertz field enhancement by a metallic nano slit operating beyond the skin-depth limit," Nat. Photonics **3**, 152–156 (2009).
7. D. J. Park, S. B. Choi, Y. H. Ahn, F. Rotermund, I. B. Sohn, Chul Kang, M. S. Jeong, and D. S. Kim, "Terahertz near-field enhancement in narrow rectangular apertures on metal film," Opt. Express **17**, 12493–12501 (2009).
8. J. Lee, K. Lee, H. Park, G. Kang, D.-H. Yu, and K. Kim, "Tubable subwavelength focusing with dispersion-engineered metamertials in the terahertz regime," Opt. Lett. **35**, 2254–2256 (2010).
9. R. Mendis and D. Grischkowsky, "Undistorted guided-wave propagation of subpicosecond terahertz pulses," Opt. Lett. **26**, 846–848 (2001).
10. T. D. Nguyen, Z. V. Vardeny, and A. Nahata, "Concentration of terahertz radiation through a conically tapered aperture," Opt. Express **18**, 25441–25448 (2010).
11. M. Theuer, S. Sree Harsha, and D. Grischkowsky, "Flare coupled metal parallel-plate waveguides for high resolution terahertz time-domain spectroscopy," J. Appl. Phys. **108**, 113105 (2010).
12. S.-H. Kim, E. S. Lee, Y. B. Ji, and T.-I. Jeon, "Improvement of THz coupling using a tapered parallel-plate waveguide," Opt. Express **18**, 1289–1295 (2010).

#162470 - $15.00 USD Received 7 Feb 2012; revised 21 Mar 2012; accepted 21 Mar 2012; published 26 Mar 2012

13. H. Zhan, R. Mendis, and D. M. Mittleman, "Superfocusing terahertz waves below $\lambda/250$ using plasmonic parallel-plate waveguides," Opt. Express **18**, 9643–9650 (2010).
14. H. Zhan, R. Mendis, and D. M. Mittleman, "Characterization of the terahertz near-field output of parallel-plate waveguides," J. Opt. Soc. Am. B **28**, 558–566 (2011).
15. A. Rusina, M. Durach, K. A. Nelson, and M. I. Stockman, "Nanoconcentration of terahertz radiation in plasmonic waveguides," Opt. Express **16**, 18576–18589 (2008).
16. M. Schnell, P. Alonso-Gonzalez, L. Arzubiaga, F. Casanova, L.E. Hueso, A. Chuvilin, and R. Hillebrand, "Nanofocusing of mid-infrared energy with tapered transmission lines," Nat. Photonics **5**, 283–287 (2011).
17. I.-Y Park, S. Kim, J. Choi, D.-H Lee, Y.-J Kim, M. F. Kling, M. I. Stockman, and S.-W. Kim, "Plasmonic generation of ultrashort extreme-ultraviolet light pulses," Nat. Photonics **5**, 677–681 (2011).
18. M. C. Hoffmann and J. A. Fulop, "Intense ultrashort terahertz pulses: generation and applications," J. Phys. D Appl. Phys. **44**, 08300 (2011).
19. R. Paschotta, *Encyclopedia of Laser Physics and Technology* (Wiley, 2008).
20. S. Ramo, J. R. Whinnery, and T. V. Duzer, *Field and Waves in Communications*, 3rd ed. (Wiley, 1993).
21. C.A. Balanis, *Advanced Engineering Electromagnetics* (Wiley, 1989).
22. K. Iwaszczuk, A. Andryieuski, A. Lavrinenko, X.-C. Zhang, and P. U. Jepsen, "Non-invasive terahertz field imaging inside parallel plate waveguides," Appl. Phys. Lett **99**, 071113 (2011).
23. Q. Wu and X.-C. Zhang, "Free-space electro-optic sampling of terahertz beams," Appl. Phys. Lett. **67**, 3523–33525 (1995).
24. P. Uhd Jepsen, C. Winnewisser, M. Schall, V. Schyja, S. R. Keiding, and H. Helm, "Detection of THz pulses by phase retardation in lithium tantalate," Phys. Rev. E **53**, R3052–R3054 (1996).
25. A. Nahata, D. H. Auston, T. F. Heinz, and C. Wu, "Coherent detection of freely propagating terahertz radiation by electro-optic sampling," Appl. Phys. Lett. **68**, 150 (1996).
26. Y. Berozashvili, S. Machavariani, A. Natsvlishvili, and A. Chirakadze. "Dispersion of the linear electro-optic coefficients and the non-linear susceptibility in GaP," J. Phys. D: Appl. Phys. **22**, 682 (1989).
27. N. Karpowicz, J. Dai, X. Lu, Y. Chen, M. Yamaguchi, H. Zhao, X.-C. Zhang, L. Zhang, Cu. Zhang, M. Price-Gallagher, C. Fletcher, O. Mamer, A. Lesimple, and K. Johnson. "Coherent heterodyne time-domain spectrometry covering the entire terahertz gap," Appl. Phys. Lett. **92**, 011131 (2008).

1. Introduction

Terahertz (THz) radiation allows for analysis of various properties of materials, including for example electronic states in semiconductors, dielectric properties of glasses and plastics, and vibrational modes of crystals [1, 2]. In some cases, sensing applications require detection of small amounts of substances, and thus a tight confinement of the radiation to the volume of the sample would be advantageous. In classical free-space wave optics the confinement of the electromagnetic wave is lower-limited by diffraction effects to approximately $\lambda/2$. It has been recently shown that this limitation can be overcome by use of plasmonic structures and metamaterials [3–8]. A significant effort in achieving deep subwavelength confinement has been focused on the use of tapered waveguides [9–15]. Zhan *et al.* [13] demonstrated that a tapered parallel plate waveguide (TPPWG) supports superfocusing of THz waves below $\lambda/250$. In this scheme the wave confinement is limited by the skin depth of radiation in the metal [15] and beam spots as small as 60 nm were demonstrated for tapered transmission lines illuminated with 10 μm radiation [16]. Tapering leads to compression of the electromagnetic energy carried by the electromagnetic wave, and in this way opens doors for significant field enhancement.

In this paper we investigate the field enhancement properties of a TPPWG. The paper is organized in the following way. In section 2 we describe the experimental setup and we give detailed information about the waveguide. In section 3 we develop a simple analytical approach to the estimation of the THz electric field enhancement inside a TPPWG. A full-wave numerical time-domain simulation of THz wave propagation is compared with the analytical estimation. Next two independent experimental methods, free-space electro-optic sampling (FSEOS) and air biased coherent detection (ABCD), are then used to measure the THz electric field at the output of the waveguide. The two experimental methods are compared with each other and with the numerical simulations.

#162470 - $15.00 USD Received 7 Feb 2012; revised 21 Mar 2012; accepted 21 Mar 2012; published 26 Mar 2012

2. Experimental setup

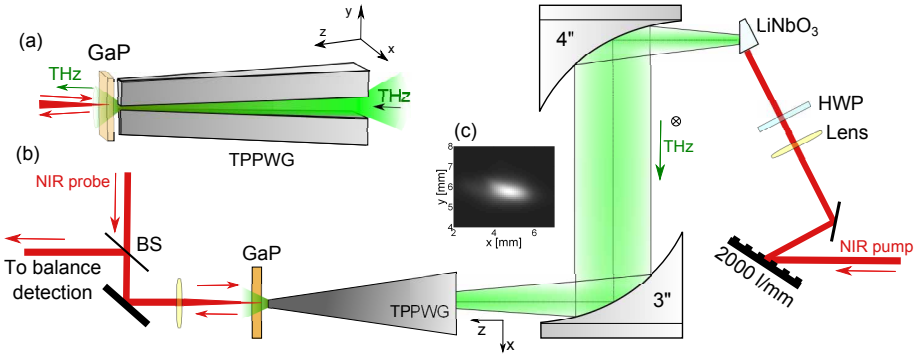

Fig. 1. (a) Schematic of the tapered parallel plate waveguide, consisting of two aluminum plates of a varying width (input 3 mm, output 49 μm) and adjustable plate separation (1 mm at the input and between 0 μm and 500 μm at the output). (b) Setup for THz wave focussing inside TPPWG. THz radiation is generated using the tilted wavefront method in $LiNbO_3$, coupled into the TPPWG, propagates along it, couples out and is detected in a 300 μm-thick [110] GaP crystal in reflection configuration. Distance between output of TPPWG and the GaP crystal is $\sim$ 360 μm. HWP - half wave plate. (c) Intensity distributions of the THz spot at the input to the TPPWG measured using a pyroelectric detector with a 250 μm-diameter aperture. The THz beam has elliptical shape with FWHMs of 1.6 mm along x-direction and 0.7 mm along y-direction.

Figure 1 shows the schematics of the experimental setup. The TPPWG consists of two electrically isolated, fine polished aluminum plates of varying width (input 3 mm, output 49 μm) and adjustable plate separation. The plate separation B_{in} at the input facet of the waveguide is set to 1 mm, while the output plate separation B_{out} can be varied between 0 and 500 μm by a micrometric stage. Aluminum was chosen as material for the waveguide plates because of its combination of high electrical conductivity and mechanical hardness, needed for low propagation loss and for the manufacturing of narrow and well-defined tips. The total length of the TPPWG is 25.4 mm. Strong broadband THz pulses are generated by tilted pulsefront optical rectification in $LiNbO_3$ [18] using near-infrared (NIR) 0.6 mJ pump pulse from a 1 kHz, 90 fs, 800 nm regenerative Ti:sapphire femtosecond laser amplifier (Spectra-Physics Hurricane). The intensity front of fs pulses is tilted by a 2000 line/mm holographic grating and imaged by a 63 mm-focal length lens with demagnification factor of 2 onto the front surface of a stoichiometric $LiNbO_3$ crystal at room temperature. THz pulse energies up to 0.5 μJ were measured directly after the $LiNbO_3$ with a calibrated pyroelectric detector. A pair of 50.8 mm-diameter, 101.6 mm and 76.2 mm focal length off-axis parabolic mirrors is used to collimate and focus the THz radiation at the input of the TPPWG. A pyroelectric detector with a 0.25 mm-diameter aperture mounted on an x-y motorized translation stage was used to image the THz field intensity distribution at the input plane of the waveguide. The THz beam has an elliptical shape, as shown in Fig. 1(c), with intensity FWHM of 1.6 mm along the x-direction and 0.7 mm along the y-direction. The THz wave couples into the TPPWG, propagates between the aluminium plates in the fundamental TEM mode and then couples out into free space at the narrow exit facet of the waveguide. Attenuated NIR probe pulses from the same laser amplifier are focused using a 50 mm-focal length lens onto a 300 μm-thick [110] gallium phosphide (GaP) crystal. The NIR probe enters the GaP crystal and is reflected from the back surface of the electro-optic crystal and then copropagates with the THz pulse. The beam waist at the focus point has been

#162470 - $15.00 USD Received 7 Feb 2012; revised 21 Mar 2012; accepted 21 Mar 2012; published 26 Mar 2012

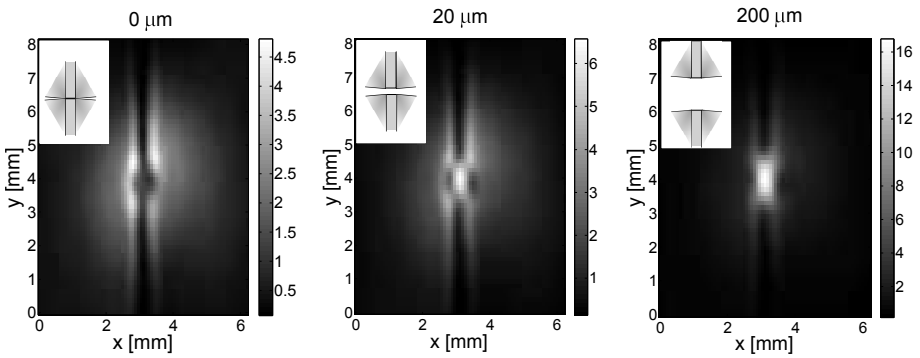

Fig. 2. Output intensity distributions measured using a pyroelectric detector with a 0.25 mm-diameter aperture placed 0.8 mm away from the waveguide tip for output gaps B_{out} of 0 μm, 20 μm and 200 μm. $B_{in} = 1$ mm.

estimated to be approximately 20 μm. The lens is mounted on a micrometric x-y-z translation stage for accurate alignment of the focus spot on the GaP crystal. Due to geometrical restrictions the distance between GaP crystal and waveguide output cannot be shorter than 300 μm. The THz electric field induces a phase retardation between polarization components of the NIR probe. This phase retardation is measured by the balanced detection. The same setup was used to detect THz field at the input plane of the waveguide.

Figure 2 shows the output intensity distributions of the THz electric field measured using a pyroelectric detector placed 0.8 mm away from the waveguide tip for output gaps of 0 μm, 20 μm and 200 μm with the input gap B_{in} = 1 mm. For the closed waveguide no THz field is transmitted directly through the output. The blurred halo observed around the center of the scan is THz waves that have leaked around the waveguide tip. The vertical lines visible in the picture are THz waves that propagate on the outside vertical walls of the waveguide. For the open gaps the major part of the THz wave propagates through the gap and dominates the pictures. These strong bursts of THz radiation, even for output gaps that are more than one order of magnitude smaller than the THz wavelength, indicate that high THz intensities are focused well below the diffraction limit.

3. Analytical and numerical field estimation

First we present a simple analytical estimation of the field enhancement at the output of the TP-PWG. In the case of illumination of the waveguide with a Gaussian elliptical beam (as depicted in Fig. 1(c)), the THz electric field $E(z)$ along the waveguide can be expressed by

$$E(z) = E_0 \cdot C \cdot FE(z). \tag{1}$$

where E_0 is the peak electric field of the Gaussian input mode at the entrance of the waveguide, $FE(z)$ is the field enhancement, and C is the coupling constant between the Gaussian input excitation beam $E_G(x,y)$ and the uniform field distribution $E_U(x,y)$ of the TEM eigenmode of the TPPWG at the input of the waveguide. The coupling constant C can be calculated using the mode overlap integral [19]:

$$C = \frac{\left|\int E_G(x,y) E_U^*(x,y)\, dA\right|}{\sqrt{\int |E_G(x,y)|^2 dA}\sqrt{\int |E_U(x,y)|^2 dA}}, \tag{2}$$

For the elliptical Gaussian beam with intensity FWHM of 1.6 mm and 0.7 mm and a uniform TEM mode, the coupling constant C has been calculated to be 0.877.

#162470 - $15.00 USD Received 7 Feb 2012; revised 21 Mar 2012; accepted 21 Mar 2012; published 26 Mar 2012

The field enhancement $FE(z)$ along the waveguide is determined by two main factors: energy squeezing due to geometrical wave confinement and propagation losses due to finite conductivity of the metal. Assuming, for simplicity, the absence of radiation losses and that the uniform TEM mode profile is sustained during wave propagation, and that the whole electric field is confined within the volume between waveguide plates, we can write that $E^2(z)A(z)/Z_{WG}(z) = E^2(z)W(z)B(z)/Z_{WG}(z) = const$, where $E(z)$, $A(z)$, $Z_{WG}(z)$, $W(z)$ and $B(z)$ are the electric field, cross-sectional area of the waveguide, impedance of the waveguide, its width and plate separation, respectively. By neglecting changes of impedance along the waveguide (which is reasonable since $Z_{in} \approx 126\ \Omega$ and $Z_{out} \approx 153\ \Omega$ for $B_{out} = 20\ \mu$m, calculated using $Z_{WG} = 120\pi b/w$ [20]) and by taking the logarithm of the last equation, we get

$$2\ln(E) + \ln(B) + \ln(W) = \ln(C). \tag{3}$$

Differentiating both sides we derive a differential equation for the THz electric field squeezing:

$$\frac{dE}{E} = -\frac{1}{2}\left(\frac{dW}{W} + \frac{dB}{B}\right). \tag{4}$$

In the case of our tapered parallel plate waveguide the width W and plate separation B are linear functions of position along the waveguide

$$W(z) = W_{in} - \frac{W_{in} - W_{out}}{L_{\mathrm{WG}}} z, \tag{5}$$

$$B(z) = B_{in} - \frac{B_{in} - B_{out}}{L_{\mathrm{WG}}} z, \tag{6}$$

where W_{in}, B_{in}, W_{out}, B_{out} are waveguide width and plate separation at the input and the output of the waveguide. L_{WG} is the total length of the waveguide. Also the decrease of the THz field due to Ohmic losses can be described by a differential equation:

$$dE = -\frac{\alpha(z)}{2} E(z)\, dz, \tag{7}$$

where α is the attenuation constant for the TEM mode and can be expressed by [21]

$$\alpha(z) = \frac{2nR_s}{Z_0 B}. \tag{8}$$

$R_s = \sqrt{\pi f \mu/\sigma}$ is the waveguide surface resistivity, n is the refractive index of the material filling the waveguide, Z_0 is the free space impedance and σ is the electrical conductivity of the metal. The final equation describing the field evolution in this simple model is a sum of Eq. (4) and Eq. (7).

$$\frac{dE}{E} = -\frac{\alpha}{2} dz - \frac{1}{2}\left(\frac{dW}{W} + \frac{dB}{B}\right). \tag{9}$$

Integrating this equation with the width and plate separation coordinate dependence given by Eq. (5) and Eq. (6), and inserting the solution into Eq. (1), we get an expression for the electric field along the waveguide,

$$E(z) = E_0 \cdot C \cdot \sqrt{\frac{W_{in}B_{in}}{W(z)B(z)}} \cdot \left[1 - \left(1 - \frac{B_{out}}{B_{in}}\right)\frac{z}{L_{\mathrm{WG}}}\right]^{\frac{R_s}{Z_0}\frac{L_{\mathrm{WG}}}{B_{in}-B_{out}}}. \tag{10}$$

The term $FS = \sqrt{\frac{W_{in}B_{in}}{W(z)B(z)}}$ describes the field squeezing due to geometrical restrictions, while the second term, which we will call field reduction FR, is attributed to the conduction losses inside the metal.

#162470 - $15.00 USD Received 7 Feb 2012; revised 21 Mar 2012; accepted 21 Mar 2012; published 26 Mar 2012

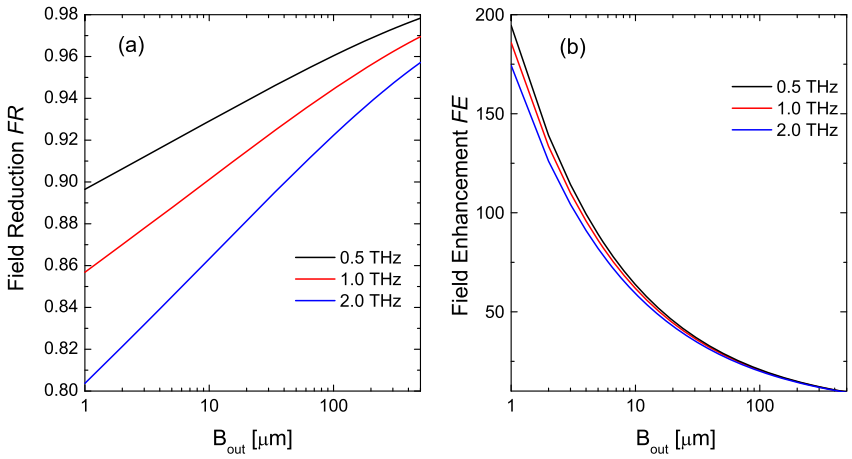

Fig. 3. (a) Calculated field reduction *FR* due to ohmic losses at the output of a TPPWG as a function of the output gap B_{out} for 0.5, 1.0 and 2.0 THz. (b) Calculated field enhancement $FE = E(L)/E_0$ at the output of a 2D-tapered PPWG as a function of the output gap B_{out} for 0.5, 1.0 and 2.0 THz. The field enhancement is achieved by energy squeezing in the area between metal plates and is corrected by ohmic losses. Data for input plate spacing $B_{in} = 1000\ \mu$m, the total length of the waveguide $L_{\mathrm{WG}} = 25.4$ mm and conductivity of the metal $\sigma = 3.56 \cdot 10^7$ S/m.

Figure 3(a) shows the calculated field reduction *FR* at the output of a TPPWG as a function of the output gap B_{out} for the field frequencies of 0.5, 1.0 and 2.0 THz. It can be seen in the figure that the field reduction depends strongly on the output plate separation B_{out}, in a way that the larger the plate separation the smaller the losses. Hence the attenuation coefficient α increases with the frequency of the propagating THz field as a $\sqrt{f}$, therefore the field reduction *FR* is also frequency dependent. Figure 3(b) shows the field enhancement $FE = E(L)/E_0$ at the output of the TPPWG, calculated using Eq. (10). The field enhancement increases with decreasing output plate separation. For B_{out} smaller than 20 μm values of *FE* above 45 are achieved. The presented calculations account neither for diffraction losses nor reflection from the non-perfect impedance matching, and therefore the actual values of *FE* will be lower. The derivation of Eq. (10) also does not take into account that the mode profile of the guided wave may depend on plate width and separation.

The time-domain numerical simulations are performed with CST Microwave Studio for a full size TPPWG made of aluminium treated as a lossy metal. The TPPWG is meshed with $40 \cdot 10^6$ mesh cells. Perfectly matched layer (PML) boundary conditions are used. Simulations are performed on a 12-core processor workstation with 48 GB of memory and each requires ~ 4.5 hours of computing time. The THz beam at the input to the waveguide has elliptical Gaussian shape, with intensity FWHM of 1.6 mm along x-direction and 0.7 mm along y-direction, as determined in our experiments. The THz time waveform measured at the input faced of the waveguide was used for simulation. Figure 4 shows the peak electric field at the central point between the metal plates along the TPPWG for output gaps B_{out} of 20, 40, 60, 100, 140 and 200 μm. The electric field is normalized to the maximum of the Gaussian field at the input to the waveguide. The input of the waveguide is at $z = -25.4$ mm and the output is at $z = 0.0$ mm. During the first 7 mm of the waveguide the THz peak electric field oscillates. Those changes are likely caused by the mode conversion between the free-space Gaussian mode and the TEM mode of finite-width waveguide. In the last 18 mm of the TPPWG we observe a

#162470 - $15.00 USD Received 7 Feb 2012; revised 21 Mar 2012; accepted 21 Mar 2012; published 26 Mar 2012

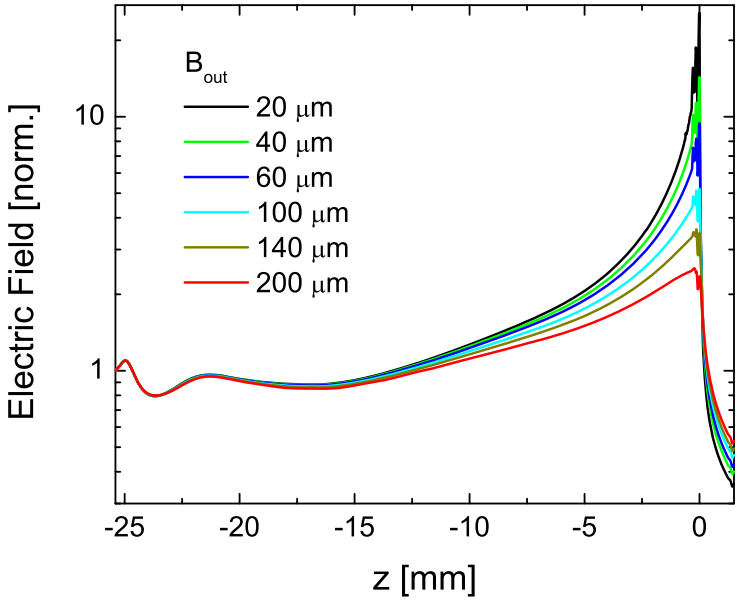

Fig. 4. Simulated peak electric field along the TPPWG for output gaps B_{out} of 20, 40, 60, 100, 140 and 200 μm. Electric field is normalized to the field at the input to the waveguide. Field values for the center points between plates. Input to the waveguide is at $z = -25.4$ mm and the output at $z = 0.0$ mm. Data for $B_{in} = 1000$ μm, $W_{in} = 3000$ μm, $W_{out} = 49$ μm, $L_{\mathrm{WG}} = 25.4$ mm and conductivity of the metal $\sigma = 3.56 \cdot 10^7$ S/m.

gradual increase of the peak THz electric field. A field enhancement higher than a factor of 20 is achieved for the output gap of 20 μm. As the THz wave arrives at the output facet of the TPPWG part of it is reflected due to the impedance mismatch between the waveguide and free space. The interference between the incident and reflected wave causes oscillations of the peak THz electric field observed in vicinity of the waveguide output [22]. At $z = 0$ mm THz field couples out of the TPPWG, and for $z > 0$ mm the peak electric field decreases due to strong diffraction. The smaller the output gap the bigger the diffraction angle in the vertical direction and therefore the faster the decrease of the peak electric field. Also the reflection coefficient is larger for smaller gaps, so less energy couples out when B_{out} is narrow.

Figure 5 shows the calculated cross-sectional distributions of the y-component of the peak THz electric field along the TPPWG for few chosen positions z. The field at the input ($z = -25.1$ mm) of the waveguide has an elliptical gaussian distribution. The general trend visible from the presented field distributions is that the major part of the energy of the THz field is confined within the area between metal plates. The confinement is tighter for smaller plate separations. At the position of $z = -9.1$ mm the field has a distribution more resembling the uniform field distribution of the TEM mode, except in the proximity of the edges of the waveguide, where it is enhanced. This effect has previously been reported by Zhan *et al.* [13], and can be explained by the presence of propagating edge plasmons. Once the THz transient couples out of the TPPWG the THz beam rapidly diffracts. In Fig. 5(j) we see a blurred halo around the center of the image and the vertical lines that originate from the THz waves that propagate on the outside vertical walls of the waveguide, in close agreement with the measurements shown in Figs. 2(a) and 2(b).

#162470 - $15.00 USD Received 7 Feb 2012; revised 21 Mar 2012; accepted 21 Mar 2012; published 26 Mar 2012

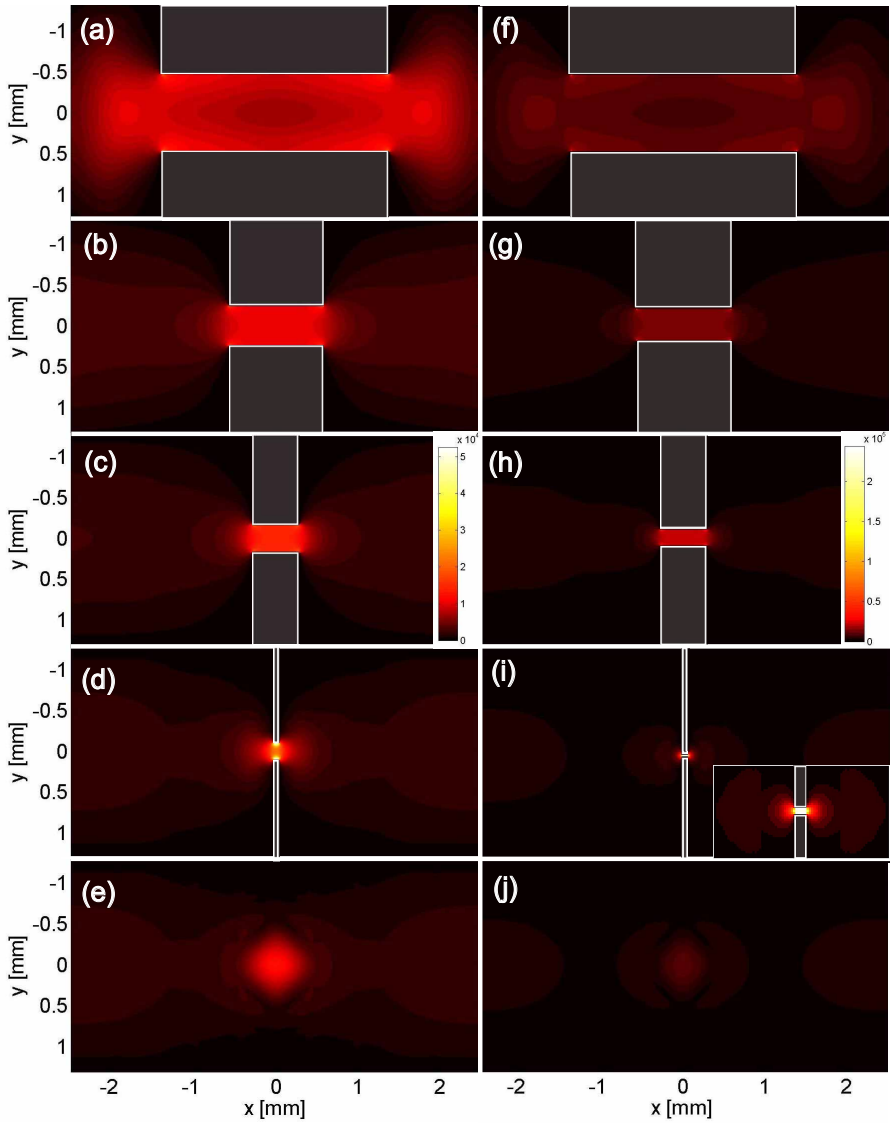

Fig. 5. Distributions of the y-component of the peak THz electric field along the TPPWG for B_{out} of (a-e) 200 μm and (f-j) 20 μm at positions along the waveguide z = −25.1, −9.1, −4.1, −0.1 and 0.9 mm. Note that scales in the left and right column are different (left column range is 0 to 20.000 V/m, right column range is 0 to 100.000 V/m).

#162470 - $15.00 USD Received 7 Feb 2012; revised 21 Mar 2012; accepted 21 Mar 2012; published 26 Mar 2012

Figure 6 shows the ratio between the THz field enhancement simulated using CST Microwave Studio (FE_{sim}) and calculated analytically (FE_{an}) using Eq. (10), at the output of the TPPWG for different sizes of the output gap B_{out}. The main difference between FE_{sim} and FE_{an} is that the analytical quantity does not account for radiation losses, so $\frac{FE_{sim}}{FE_{an}}$ is a good representation of radiation losses during propagation along the TPPWG. It is clear from the Fig. 5 that diffraction losses increase with increasing output gap separation. This effect can be explained using the contrast between the effective waveguide impedance Z_{WG} and the free space impedance Z_0. Narrowing the plate separation increases the effective waveguide impedance Z_{WG}. Higher contrast between Z_{WG} and Z_0 leads to higher reflection coefficient in the x-direction, which means that the THz wave is tighter confined within the waveguide. This effect is analogous to solid core optical fibers, where high contrast in refractive index gives tight confinement of the optical wave. An exponential function fits the data points in Fig. 6 accurately, with parameters shown in the figure. This observation is in agreement with the work of Zhan *et al.* [13], who have shown experimentally that the field confinement in the area between the plates of a PPWG decreases exponentially with increasing plate separation.

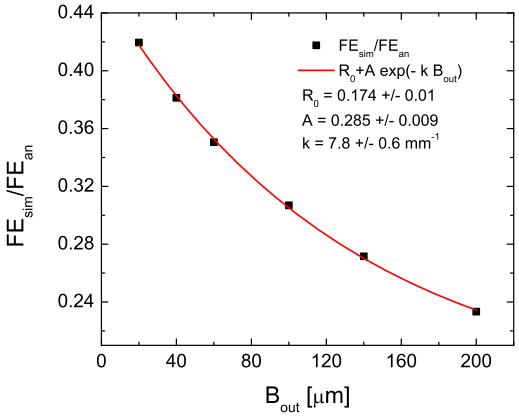

Fig. 6. Calculated diffraction losses in a TPPWG as a function of the output gap B_{out} for a THz wave at 1.0 THz. Solid line shows exponential fit. Data for $B_{in} = 1000\ \mu$m, $W_{in} = 3000\ \mu$m, $W_{out} = 49\ \mu$m, $L_{\mathrm{WG}} = 25.4$ mm and conductivity of the metal $\sigma = 3.56 \cdot 10^7$ S/m.

4. THz electric field calibration

To experimentally quantify the predicted THz field enhancement in the TPPWG, two independent methods are used. The first method is to detect THz radiation using free space electro-optic (EO) sampling [23–25] outside the TPPWG, as shown in Fig. 1(b), and then to use outcoupling coefficients, delivered by numerical simulation, to compute the field strengths at the output of the waveguide. In the EO detection the THz electric field was calculated using the equation $E_{THz} = \frac{\Delta I}{I_0} \frac{c}{\omega n_0^3 r_{41} L}$, where $\frac{\Delta I}{I_0}$ is the modulation depth of the light intensity in the balance detection, ω is the center frequency of the NIR probe, n_0 is the refractive index of the EO crystal, L is its thickness and r_{41} is the electro-optic coefficient of the [110] GaP crystal (0.88 pm/V [26]). Figure 7(a) shows waveforms of THz radiation transmitted through the TPPWG for various output plate separation B_{out}. THz radiation is detected in 300 μm-thick [110] GaP crystal positioned $\sim 360\ \mu$m away from the waveguide output. The previously described numerical CST Microwave Studio simulations were used to obtain values of the outcoupling coefficients,

#162470 - $15.00 USD Received 7 Feb 2012; revised 21 Mar 2012; accepted 21 Mar 2012; published 26 Mar 2012

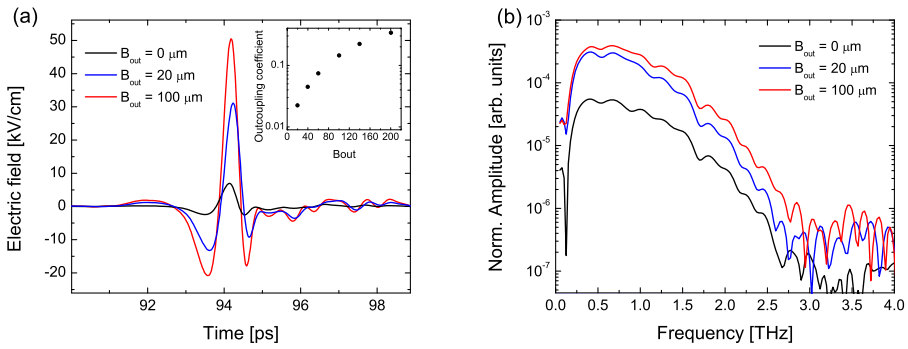

Fig. 7. (a) THz waveforms of radiation transmitted through the TPPWG for various output plate separation B_{out}. THz radiation is detected in 300 μm-thick [110] GaP crystal positioned $\sim$ 360 μm away from the waveguide output. Inset shows field outcoupling coefficients, calculated using numerical simulation. (b) Amplitude spectra for various output plate separation B_{out}.

presented in the inset to Fig. 7(a). Outcoupling coefficients are calculated by considering the average of the peak THz electric field over the length of the GaP crystal divided by the peak value of the field at the tip of the waveguide. Figure 7(b) shows the amplitude spectra of the detected THz radiation obtained from a Fourier transform. The amplitude spectrum extends from 0.1 THz up to 2.5 THz. Dips in the spectra are due to absorption of THz radiation by water vapor in the air.

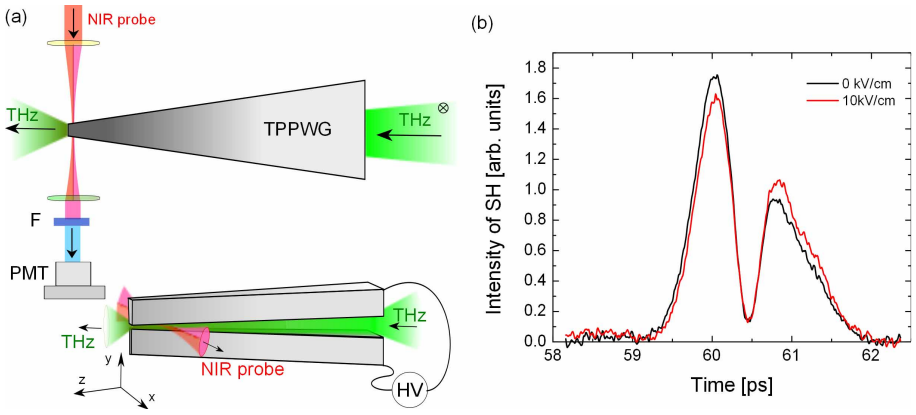

Fig. 8. (a) Schematic of the air photonic setup for THz field measurement inside a tapered parallel plate waveguide. THz radiation coupld into the TPPWG, propagates along it and interacts with NIR probe inducing second harmonic generation. F - 400 nm bandpass filter, HV - high voltage source, PMT - photomultiplying tube. (b) Time dependent intensity of THz induced second harmonic (SH) for an output gap of 100 μm with and without DC bias.

The second method for calibrating the electric field strength of the THz wave at the output of the TPPWG is based on the air-photonic measurement the THz induced second harmonic (SH) intensity [22]. Figure 8(a) shows the simplified schematics of the air photonic setup for THz field measurement inside a tapered parallel plate waveguide. A high voltage source is connected to the waveguide plates and can deliver an electric bias field between the metal plates. A NIR

#162470 - $15.00 USD Received 7 Feb 2012; revised 21 Mar 2012; accepted 21 Mar 2012; published 26 Mar 2012

beam from the same laser amplifier as used for THz generation is used for probing the THz field. The probe beam is focused in the center of the volume between the plates with a 19 mm-focal length lens and recollimated after the waveguide. The beam is sent through 400 nm bandpass filters and then to a photomultiplier tube (PMT) which detects the 400-nm light generated in the nonlinear process. The signal from the PMT is measured by a lock-in amplifier referenced to an optical chopper modulating the THz beam. The polarizations of the four interacting electric fields (terahertz, fundamental, second harmonic and bias) are perpendicular to the waveguide plates. Further experimental details concerning setup are presented elsewhere [22]. According to Karpowicz *et al.* [27] the interaction between the laser NIR pulse (intensity I_ω) and the THz electric field E_{THz} in the presence of the external electric field E_{bias} leads to generation of a second harmonic beam with intensity $I_{2\omega}$ of

$$I_{2\omega} \propto \left(\chi^{(3)}_{xxxx} I_\omega\right)^2 \left[E^2_{THz} + 2E_{bias}E_{THz} + E^2_{bias}\right]. \tag{11}$$

where $\chi^{(3)}_{xxxx}$ is the third-order nonlinear susceptibility of the air. If an optical chopper is modulating the THz beam, a lock-in amplifier referenced to the chopper frequency detects following SH intensity

$$I_{2\omega} \propto [E^2_{THz} + 2E_{bias}E_{THz}]. \tag{12}$$

If two measurements of SH intensity ($I^0_{2\omega}$ without and $I^{bias}_{2\omega}$ with known external DC bias) are performed, then the absolute amplitude and sign of the THz electric field can be determined:

$$I_{mod} = \frac{I^{bias}_{2\omega} - I^0_{2\omega}}{I^0_{2\omega}} = \frac{2E_{bias}E_{THz}}{E^2_{THz}}, \tag{13}$$

$$E_{THz} = \frac{2E_{bias}}{I_{mod}}, \tag{14}$$

where I_{mod} is the relative modulation depth of the generated second harmonic. Figure 8(b) shows measured intensity of the time-dependent THz induced SH without and with external 10 kV/cm bias at the output of TPPWG with an output gap of 100 μm. Because of the bipolar shape of the single-cycle THz transient [Fig. 7(a)] of the THz transient one peak of the induced SH decreases in the presence of the external bias field while the other one increases. Using the method outlined above, the peak of the THz electric field has been measured to be 295 kV/cm.

Figure 9 presents a summary of our measurements of the peak THz field at the output of the TPPWG for different output gaps B_{out}. Black squares are the results of the direct measurement using THz-induced second harmonic generation. Unfortunately, due to the high intensity of the probe beam (though still lower than the plasma ionization threshold), measurements of the THz field in this way for B_{out} smaller than 60 μm resulted in a high chance of damaging the waveguide, so values are presented only for $B_{out} \geq 60\mu$m. The red circles represent values of the peak THz electric field measured using electro-optic detection in GaP crystal corrected by outcoupling coefficients. The blue dashed line shows the peak values of the THz field from CST Microwave Studio simulations, using the previously described elliptical beam with the experimentally determined value of the peak THz field of 68 kV/cm as input. All the three values of the peak electric field at the tip of the TPPWG agree well with each other over a wide range of B_{out}. The small differences can have various origins. For the THz field obtained by air-photonic method they can be caused by non-uniform distribution of the bias field within the THz beam. Deviations can also come from the fact that local field enhancement at the edges of the waveguide were probed. The uncertainty of the electro-optic values are increasing with decreasing the output gap size, since the outcoupling coefficients are smaller. Error bars in the Fig. 9 are dominated by the uncertainty of the distance between the waveguide tip and GaP

#162470 - $15.00 USD Received 7 Feb 2012; revised 21 Mar 2012; accepted 21 Mar 2012; published 26 Mar 2012

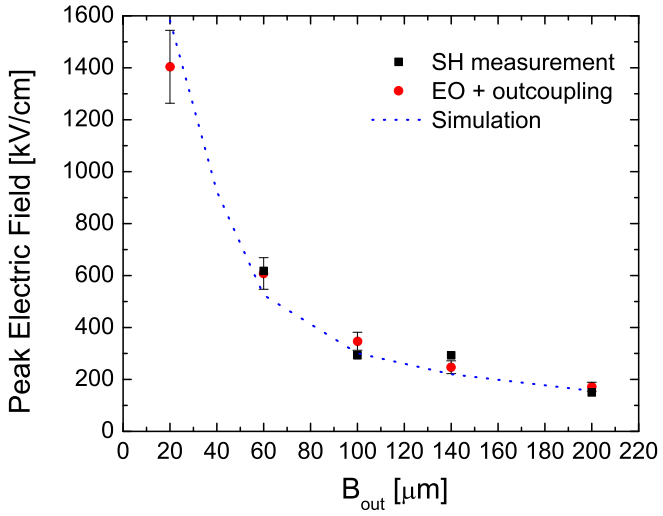

Fig. 9. Peak electric field at the output of the TPPWG for different output gaps B_{out}.

crystal. In any case the good agreement between different measurements indicate that very high values of the THz field at the tip of the waveguide were achieved. For the output gap of 20 μm we estimated a value of over 1.4 MV/cm. Even higher values are expected for smaller output gaps.

5. Conclusions

We have investigated field enhancement properties of the TPPWG and we have showed that a field enhancement of over 20 is possible, resulting in the THz peak electric field exceeding 1.4 MV/cm for output gaps of 20 μm. The field values have been measured using two methods: free-space electro-optic sampling and THz enhanced second harmonic generation. The obtained values agree with each other and also with predictions from numerical simulations. Even higher values of the peak THz field are expected for smaller output gaps. The tight concentration of high intensity THz radiation can be potentially applied in exploration of nonlinear THz phenomena, deep-subwavelength imaging, and allow for development of compact optoelectronic devices.

Acknowledgments

The authors acknowledge partial financial support of the Future and Emerging Technologies (FET) programme within the 7th Framework Programme for Research of the European Commission, under FET-Open grant number 250056 (TREASURE). We also acknowledge the Danish Council for Technical and Production Sciences (NIMbus project). X.-C. Zhang was supported in part by the Defense Threat Reduction Agency, and National Science Foundation.

#162470 - $15.00 USD Received 7 Feb 2012; revised 21 Mar 2012; accepted 21 Mar 2012; published 26 Mar 2012